ACS OMEGA

http://pubs.acs.org/journal/acsodf

Article

Reed Rhizome Residue-Based Activated Carbon Adsorption Ultrafiltration Membranes for Enhanced MB Removal

Zhen Li,* Xiongwei Luo, and Yonghong Li

Cite This: *ACS Omega* 2022, 7, 43829−43838

Read Online

ACCESS | Metrics & More | Article Recommendations | Supporting Information

ABSTRACT: Novel adsorption ultrafiltration (ADUF) membrane was designed for the removal of methylene blue (MB) by introducing Chinese herbal waste-based activated carbon (AC) into the ultrafiltration membrane. We prepared AC particles from Chinese herbal medicine waste residue (reed rhizome residue) as a raw material by $ZnCl_2$ activation and introduced them into the ultrafiltration membrane by phase inversion to prepare a reed rhizome residue-based activated carbon adsorption ultrafiltration (RAC-ADUF) membrane. The RAC-ADUF-0.1 membrane was characterized by a series of physical structures and chemical properties, which showed that the prepared membrane has a more hydrophilic surface and high porosity. The RAC-ADUF-0.1 membrane showed an excellent pure water flux of 255.77 $L{\cdot}m^{-2}{\cdot}h^{-1}$ and a high bovine serum albumin rejection of 99.3%. The RAC-ADUF membranes also possessed excellent antifouling performance. Notably, the RAC-ADUF-0.1 membrane provides excellent removal of MB (99% retention) compared to conventional ultrafiltration membranes. The static adsorption capacity was up to 238.48 mg/g. The significant increase in dynamic adsorption capacity on the RAC-ADUF membrane is due to the three-dimensional distribution of RAC particles on the PSF membrane cross section, which provides more active sites and increases the contact time between RAC and MB. By fitting the adsorption kinetics and isothermal adsorption curves, the results showed that the pseudo-second-order kinetic model and the Langmuir isothermal model were more accurate in explaining the adsorption process. Further kinetic analysis showed that the adsorption process of MB molecules on RAC-ADUF membranes is controlled by both external mass transfer and intraparticle diffusion, with intraparticle diffusion playing a dominant role. In addition, the RAC-ADUF membrane exhibited outstanding adsorption and regeneration abilities, and the MB removal rate stayed at about 95% after 8 adsorption regeneration experiments. In conclusion, this study provides a new idea for the preparation strategy of an adsorption ultrafiltration membrane with high rejection and high permeability and the reuse of Chinese herbal medicine waste residue.

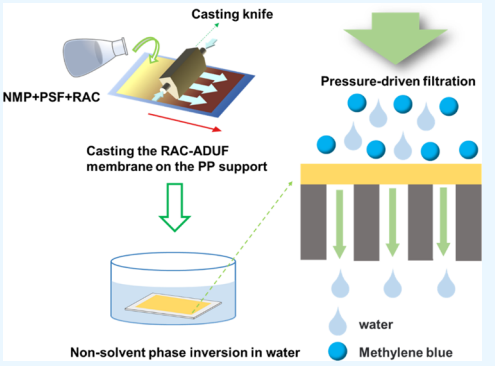

1. INTRODUCTION

With the rapid development of the textile industry, the annual production of wastewater containing dyes is about one-fifth of the total global wastewater.[1−3] Because most aromatic dye wastewater containing benzene rings is not easily degradable, toxic, and carcinogenic,[4−7] if the dye wastewater is discharged directly without treatment, it would not only hinder photosynthesis and interfere with the natural purification process of aquatic organisms but also bring irreversible damage to the human environment.[8−10] Among the many dyes, methylene blue is one of the most commonly used heterocyclic aromatic dyes and is commonly used for dyeing natural fabrics such as silk and cotton. However, methylene blue can cause lasting damage to organs (eyes, skin, etc.) in humans and animals. MB can also irritate the gastrointestinal tract and cause heart rate disorders if swallowed. Therefore, the maximum residual amount of MB in aquatic products in Japan and other countries should not exceed 10 μg/kg. Therefore, this type of aromatic dye wastewater needs to be properly treated before discharge.

At present, dye wastewater treatment methods mainly include ion exchange, ozonation, biodegradation, adsorption technology, and membrane separation technology.[4,11−16] Among these technologies, membrane separation technology and adsorption technology are widely used for wastewater treatment because of their low cost and high treatment efficiency.[17] Nanofiltration (NF) and ultrafiltration (UF) are commonly used membrane separation techniques for wastewater treatment.[5] NF technology has excessive treatment costs for low concentration and the large volume of dye wastewater due to a relatively high operating pressure.[18] Compared with NF, the operating pressure of UF technology is lower, which can reject pollutants larger than the membrane pore size,[19] but

Received: August 4, 2022
Accepted: November 3, 2022
Published: November 17, 2022

the removal effect is not ideal for pollutants smaller than the membrane size (such as small molecular organic dye). Adsorption technology is used to remove dye molecules by adding the adsorbent to the dye wastewater and adsorbing the dye molecules on its surface through physical or chemical adsorption.[11,20] Currently, the most commonly used adsorbent material is activated carbon (AC).[8,13] Many studies have focused on AC extracted from natural low-cost wastes, such as orange peels, bamboo shoots, peanut shells, and coconut shells, to remove dye pollutants from water.[12,21−23] Therefore, using natural waste to produce AC increases the economic value and reduces cost and is an ideal substitute for commercial AC. However, the problem that cannot be ignored is that the AC adsorbent is generally prepared in the form of powders and added to the water body,[24] which would make the separation process of the adsorbent material (such as high-speed centrifugation and filtration etc.) produce a large economic cost. Moreover in the process of large-scale actual operation, the loss of adsorbents is inevitable, and the loss of the powdered AC material will also have potential harm to water bodies.

To overcome the problems of powder adsorbent and ultrafiltration membrane in removing small-molecular dyes, the adsorption ultrafiltration (ADUF) membrane has attracted wide attention in the field of removing small molecular organic matter in wastewater.[25−27] The ADUF membranes can achieve efficient removal of small molecule dyes and overcome the diffusion of the adsorbent during treatment via fixing the adsorbent on the ultrafiltration membrane.[28] This strategy achieves the dual function of ultrafiltration and adsorption in one unit. Therefore, the ADUF membrane is considered one of the most efficient and competitive water reuse technologies. At present, the preparation of the ADUF membrane mainly includes physical blending and surface modification.[29,30] The physical blend is the introduction of adsorbent materials such as Fe_3O_4 nanoparticles,[31] zeolite nanoparticles,[32] and graphene oxide nanoparticles[33] into the membrane matrix to act as adsorbents for dye molecules. Unfortunately, the complex preparation process and high material price of these materials limit their large-scale use. The surface modification method is to introduce adsorption materials on the membrane surface, which cannot be ignored as it would lower the porosity and pore size of the membrane, resulting in a reduction in membrane filtration performance.[34] Therefore, improving membrane filtration and adsorption performance is a major challenge.

As mentioned above, using wastes to produce AC for the treatment of dye wastewater can increase economic value, reduce costs, and reduce waste. China is a big country in the Chinese herbal medicine production industry. With the development of the Chinese herbal medicine production industry, more than 30 million tons of Chinese herbal medicine waste residue, such as reed rhizome residue, are produced every year.[35,36] The traditional treatment methods are landfill and incineration, which not only waste resources but also pollute the environment.

Therefore, we chose reed rhizome residue as the raw material to prepare AC by $ZnCl_2$ activation, and the synthesized AC was filled into the membrane matrix by phase inversion to prepare the ADUF membrane for the efficient removal of MB. The synthesized membrane was characterized by Fourier transform infrared spectroscopy (FTIR), scanning electron microscopy (SEM), and N_2 adsorption−desorption analyses. The doping ratio of AC was optimized to achieve the simultaneous improvement of membrane filtration performance, antifouling performance, and adsorption performance of MB, and the adsorption mechanism of the ADUF membrane was clarified by fitting the adsorption kinetics and adsorption isothermal model. In addition, the regenerative capacity of the ADUF membrane was investigated.

2. EXPERIMENTAL SECTION

2.1. Materials. The reed root residue (RR) was supplied by Guangdong Lianfeng Chinese Medicine Beverage Co., Ltd; polysulfone (PSF, P S20) was supplied by BASF (Germany). Bovine serum albumin (BSA, Mw = 67 kDa) protein, *N*-methylpyrrolidone (NMP, 99.5%), polyethene glycol (PEG-400), polyethene glycol octylphenyl ether (TritonX-100), methylene blue (MB, 98%), hydrochloric acid (HCl, 1 N), zinc chloride ($ZnCl_2$, 99%), sodium chloride (NaCl, 99%), and sodium sulfate (Na_2SO_4, 99%) were purchased from Sinopharm Chemical Reagent Co. All chemical reagents used in this experiment were of analytical grade and were not further purified.

2.2. Preparation of Reed Rhizome Residue Based on Activated Carbon. In a previous study, the optimum conditions for the preparation of reed root residue activated carbon were determined using the Response surface methodology (RSM) method.[37] Specifically, 4.0 g of washed reed root residue was dipped into 40 mL of configured $ZnCl_2$ solution and mixed thoroughly, and the impregnated sample was obtained after 12 h of room-temperature impregnation and 12 h of drying (100 °C). The sample was weighed and loaded in a nickel boat and placed in a 316 stainless-steel tube reactor (SK3-5-12-6 energy-saving vacuum tube furnace from Hangzhou Zhuochi Instruments Co., Ltd.) and heated to 600 °C for 1 h under nitrogen protection to complete the charring. The obtained reed activated carbon samples were washed with a dilute hydrochloric acid solution to remove impurities such as metal ions and ash, and the samples were washed with deionized water to neutral, followed by drying, and grinding, and sieving to obtain 80 μm activated carbon powder.

2.3. Preparation of RAC-ADUF Membranes. All cast film solutions were prepared using a fixed concentration of PSF (15 wt %), PEG 400 (2 wt %), and TritonX-100 (2 wt %). The concentration of the solvent in the casting solution varies depending on the content of the RAC, which has been sieved to obtain particles with a particle size of less than 80 μm and then added to the casting solution at different additions (see Table 1). To obtain a homogeneous suspension, all components were mixed simultaneously with NMP and stirred by mixing with a magnetic stirrer (400 rpm) for 12 h and then

Table 1. Compositions of Casting Solution Used in This Study

membrane name	PSF (wt %)	PEG (wt %)	TritonX-100 (wt %)	RAC (wt %)	NMP (wt %)
PSF	15	2	2	0	81.00
RAC-ADUF-0.05	15	2	2	0.05	80.95
RAC-ADUF-0.10	15	2	2	0.10	80.90
RAC-ADUF-0.15	15	2	2	0.15	80.85
RAC-ADUF-0.20	15	2	2	0.20	80.80

https://doi.org/10.1021/acsomega.2c04968
ACS Omega 2022, 7, 43829−43838

cast onto the surface of the non-woven fabric using a casting knife with a thickness of 250 μm (see Figure 1a). The prepared membranes were then placed in a water bath for solvent/non-solvent exchange. Finally, the resulting membranes were stored in deionized water at 4 °C before use.

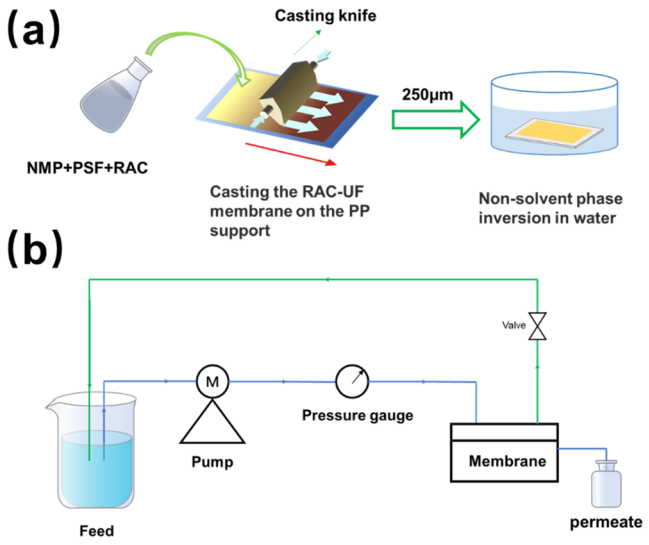

Figure 1. (a) RAC-ADUF membrane preparation process and (b) schematic diagram of membrane filtration performance testing process.

2.4. Characterization of RAC and Membranes. The top surface and cross-sectional morphology of the membranes were observed using a scanning electron microscopy (Nano-sem 430, FEI, USA). The hydrophilicity of the membrane surface was assessed using a contact angle analyzer (OCA 20LHT, datphysics). Fourier transform infrared spectroscopy attenuated total reflection (FTIR-ATR, VERTEX70, Bruker Optics) measurements were used to assess the chemical properties of the rutabagas and membranes. N_2 adsorption–desorption (ASAP-2020, Micromeritics Co. American) was used to determine the pore structure characteristics of the RAC and membranes. Zeta potentials were measured using an electrokinetic analyzer (SurPASSTM 3 Anton Paar, Austria) to determine the surface charge of the RAC-ADUF membrane.

2.5. Evaluation of Membrane Filtration Performance. The permeate flux and solute rejection of the membrane are the most important indicators for evaluating ultrafiltration membranes. In this experiment, the pure water flux and solute rejection of the membrane was measured in a homemade laboratory filtration device (Figure 1b). The effective filtration area of the membrane was 19.63 cm^2 and the specific measurement procedure was as follows: the pure water flux was measured by pre-pressurizing the membrane for half an hour at 0.15 MPa pressure, and then the pressure was adjusted to 0.1 MPa after the water flux had stabilized. The pure water flux J_0 can be calculated by the following formula

$$J_0 = \frac{V}{A\Delta t}$$

where J_0 is the pure water flux ($L{\cdot}m^{-2}{\cdot}h^{-1}$); V is the permeate volume (L); A is the effective membrane area; and Δt is the filtration time (h).

Membrane rejection was evaluated by filtration of the BSA solution. 0.1 g/L BSA phosphate buffer solution was permeated through the membrane at 0.1 MPa pressure. The absorbance of BSA in the feed solution and permeate was measured at 280 nm using a UV spectrophotometer and the corresponding concentrations were obtained

$$R = \left(\frac{C_F - C_P}{C_F}\right) \times 100\%$$

where R is the BSA retention rate; C_F is the feed fluid BSA concentration (ppm); and C_P is the permeate BSA concentration (ppm).

To reduce the experimental error, all test experiments were repeated three times and the final results were averaged.

2.6. Fouling Resistance of Membranes. The antifouling performance of RAC-ADUF and PSF membranes was investigated using BSA as a model contaminant. The membranes were filtered with pure water at 0.1 MPa for 60 min and the pure water flux J_0 was recorded. 500 mg/L BSA solution was filtered through the membranes at 0.1 MPa for 60 min to obtain the flux of J_1, and then pure water was hydraulically cleaned for 60 min to obtain the water flux of J_2. The flux recovery rate (FRR), reversible fouling ratio (R_r), irreversible fouling ratio (R_{ir}), and total fouling rate (R_t) were calculated as follows

$$FRR(\%) = \frac{J_2}{J_0} \times 100\%$$

$$R_t(\%) = \left(1 - \frac{J_1}{J_0}\right) \times 100\%$$

$$R_r(\%) = \left(\frac{J_2 - J_1}{J_0}\right) \times 100\%$$

$$R_{ir}(\%) = R_t - R_r$$

2.7. Static Adsorption Performance of MB. The effect of an initial concentration of 400 ppm (MB) in the dye solution and a solution pH in the range of 2–11 on the amount of dye adsorbed was investigated. The initial pH of all solutions was adjusted with 0.1 mol/L hydrochloric acid solution or 0.1 mol/L NaOH solution at the desired concentration.

The ionic strength experiments were carried out in the 400 ppm MB solution at pH 5, NaCl and Na_2SO_4 solution concentrations of 0.1, 0.2, 0.3, 0.4, and 0.5 mol/L.

To study the adsorption isotherm, the pH of the MB solution (pH = 5) was first adjusted using 0.5 mol/L HCl and NaOH solutions. Then, 0.25 g (membrane area 19.63 cm^2) of the membrane was placed into different concentrations of MB (100, 200, 300, 400, 600, 800, and 1000 ppm) and adsorbed for a certain time at 200 rpm oscillation speed or kept for 24 h to reach adsorption equilibrium. To gain insights into the adsorption process, the adsorption kinetics of the membranes were investigated by measuring the adsorption of MB at a concentration of 400 ppm at different adsorption times (10, 30, 60, 90, 120, 150, 180, and 210 min). Details of the relevant equations are provided in the Supporting Information.

The absorbance of MB before and after adsorption was measured by a UV spectrophotometer at 664 nm to obtain the corresponding concentration. The adsorption capacity of the membranes was calculated as follows.

https://doi.org/10.1021/acsomega.2c04968
ACS Omega 2022, 7, 43829–43838

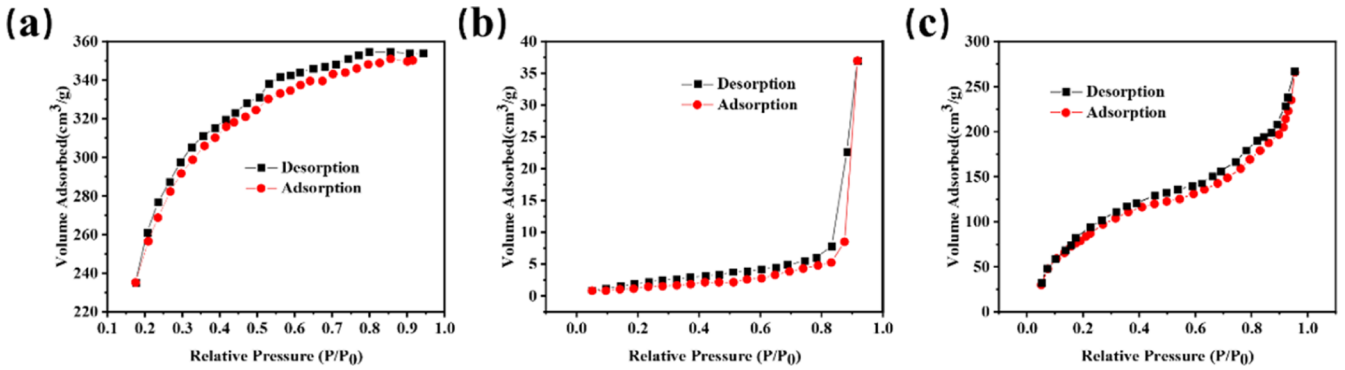

Figure 2. N_2 adsorption−desorption curves of (a) RAC, (b) PSF, and (c) RAC-ADUF-0.1 membranes.

$$q_e = \frac{(C_0 - C_e)V}{m}$$

where: q_e is the adsorption capacity (mg/g), C_0 is the initial concentration of MB (ppm), C_e is the concentration of MB at equilibrium (ppm), V is the volume of solution (mL), and m is the mass of the membrane (mg).

2.8. Removal of MB Solution by Dynamic Filtration. To investigate the actual operational performance of the RAC-ADUF membrane, MB at a concentration of 100 ppm was filtered at certain flow rates (0.526, 1.023, and 1.548 mL/min) in a homemade laboratory filtration apparatus (as shown in Figure 1b). Permeate samples were collected once every 100 mL. The concentration of MB was measured before and after filtration using a UV spectrophotometer. The MB removal of the membranes was calculated as follows.

$$R = \frac{(C_0 - C_e)}{C_0} \times 100\%$$

where: R is the MB removal (%), C_0 is the initial concentration of MB (ppm), and C_e is the concentration of MB at equilibrium (ppm).

2.9. Membrane Regeneration Performance Study. The repeated regeneration capacity of the RAC-ADUF membrane in this study was determined by multiple adsorption/desorption experiments. After each filtration and adsorption, the membranes were soaked in anhydrous ethanol for 3 h and then washed with deionized water for 1 h.[38] After washing, the regenerated membranes were repeated for filtration and adsorption of solutions containing MB under the same conditions as described above.

3. RESULTS AND DISCUSSION

3.1. Characterization of RAC-ADUF Membrane. As shown in Figure 2a−c, the pore structure characteristics of the synthesized RAC, PSF membrane, and RAC-ADUF membrane were examined using N_2 adsorption−desorption isotherms, and it can be seen in Figure 2a and Table 2 that the specific surface area and pore volume of the AC synthesized with reed rhizome residue were larger. Comparing the PSF membrane and RAC-ADUF-0.1 membrane, it can be concluded that the pore volume of the RAC-ADUF-0.1 membrane is elevated and the pore size is decreased. From Figure 2c, it can be seen that the RAC-ADUF-0.1 membrane presents the characteristics of a distinct mesoporous material. Due to the presence of RAC, the RAC-ADUF-0.1 membrane has a hysteresis loop compared with the PSF membrane. Moreover, the specific surface area and pore volume of the RAC-ADUF-0.1 membrane was significantly higher than those of the PSF membrane, which would facilitate the adsorption of MB.[39] The textural properties of RAC, RAC-ADUF-0.1, and PSF membranes are shown in Table 2.

Table 2. Textural Properties of RAC, PSF, and RAC-ADUF-0.1

sample	surface area (m^2/g)	pore volume (cm^3/g)	pore size (nm)
RAC	890.2	0.477	56.56
PSF	4.869	0.031	15.310
RAC-ADUF-0.10	265.3	0.232	13.261

Figure 3a−f shows the SEM images of the RAC, PSF membrane, and RAC-ADUF-0.1 membrane. From Figure 3a,b, it can be seen that the AC synthesized with the reed rhizome residue has a uniformly distributed pore structure on the

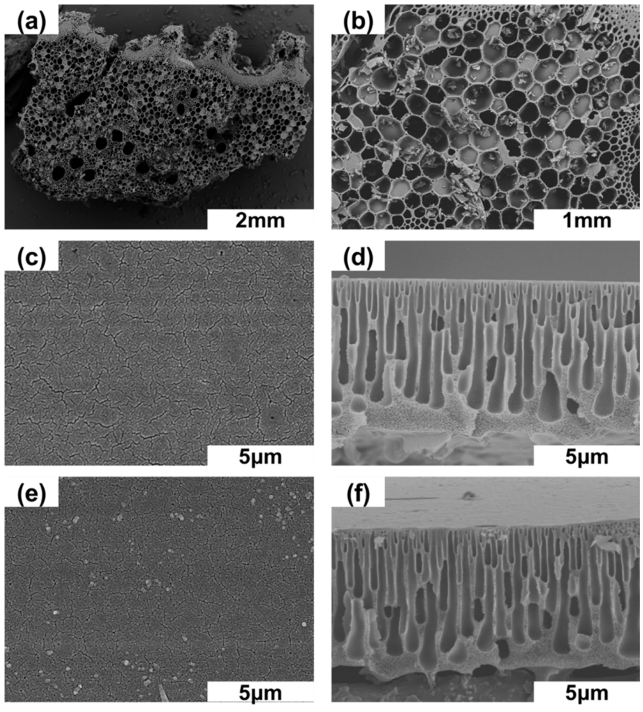

Figure 3. SEM image of RAC and UF membrane; (a,b) RAC particle; (c) PSF membrane surface and (d) cross-section; and (e) RAC-ADUF-0.1 surface and (f) cross-section.

https://doi.org/10.1021/acsomega.2c04968
ACS Omega 2022, 7, 43829−43838

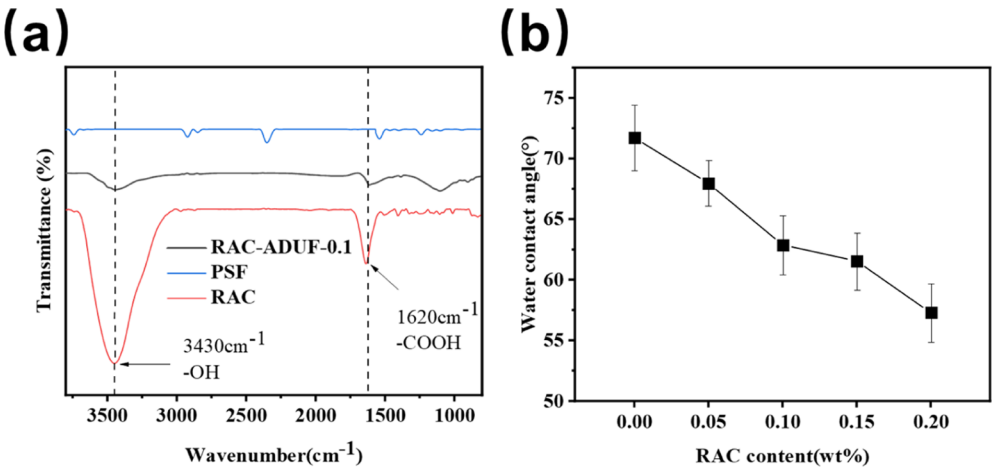

Figure 4. (a) FTIR results of RAC, PSF membrane, and RAC-ADUF-0.1 membrane and (b) WCA of PSF membrane and RAC-ADUF membranes.

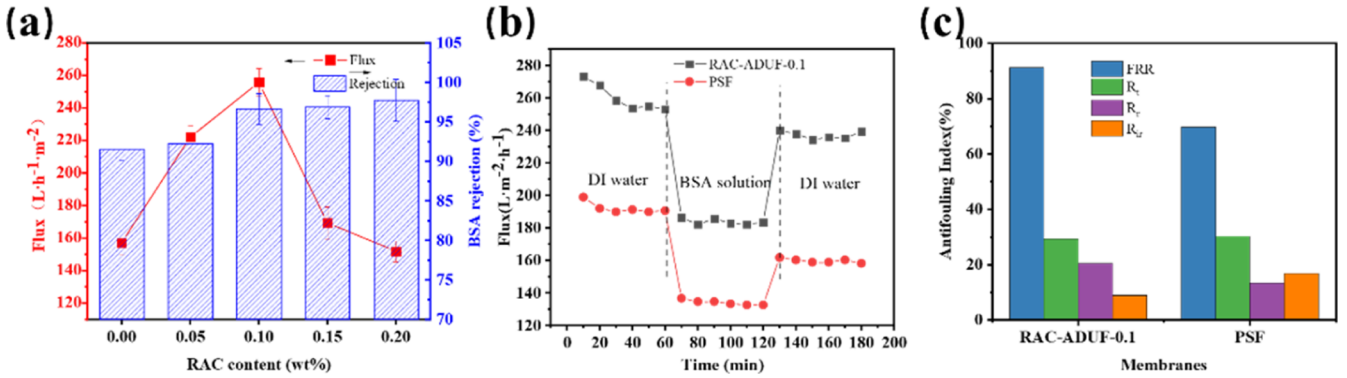

Figure 5. (a) Effects of RAC contents in the casting solution on membrane performance; (b) time-dependent flux of the RAC-ADUF-0.1 membrane under one filtration cycle; and (c) antifouling index of RAC-ADUF-0.1 membrane and PSF membrane.

surface. This indicates that the AC prepared by using reed rhizome residue can be used as an ideal adsorbent material. Comparing Figure 3c,e, it can be seen that when RAC was added, the membrane surface was slightly protruded, which was caused by the high viscosity of the membrane casting solution.[40] Comparing Figure 3d,f, the addition of RAC limits the formation of finger-like macropores during the phase inversion. In addition, it can also be learned from Table 2 that the porosity of the RAC-ADUF-0.1 membrane was increased by 20% compared to the PSF membrane, indicating that the porous structure of the RAC-ADUF-0.1 membrane was more pronounced. In addition, the RAC-ADUF-0.1 membrane contains more finger holes at the top of the membrane unlike the large holes at the bottom of the PSF membrane. The pore structure of the RAC-ADUF-0.1 membrane is beneficial to reduce mass transfer and improve membrane flux and reduce membrane surface fouling.

The chemical properties of the functional groups of RAC, PSF membrane, and RAC-ADUF-0.1 membrane are exemplified in Figure 4a. It can be seen that the synthesized RAC particles have a large number of hydrophilic functional groups (−OH and −COOH). Compared to the PSF membrane, the RAC-ADUF-0.1 membrane has characteristic peaks at 3430 cm^{-1} (−OH) and 1639 cm^{-1} (−COOH).[41] It indicates that the introduction of RAC into the PSF membrane matrix resulted in the appearance of a large number of hydrophilic hydroxyl (−OH) and carboxyl (−COOH) groups on the PSF membrane surface,[42,43] which can facilitate reinforcement of the water flux and antifouling performance of the membrane and can be discussed intimately within the later section.

The hydrophilicity of the membrane is an important factor influencing its flux and anti-fouling performance.[44] We measured the WCA of the membrane to determine its hydrophilicity. From Figure 4b, the WCA dramatically lowers following the inclusion of RAC in the PSF membrane, and it further decreases with increasing RAC content. The FTIR results show that by introducing RAC, a high number of hydrophilic hydroxyl and carboxyl groups form on the PSF membrane surface, considerably enhancing the hydrophilicity of the PSF membrane and will hopefully achieve the goal of improving the water flux.[41]

3.2. Performance of RAC-ADUF Membranes. Figure 5a depicts the pure water flows and BSA rejection of PSF and RAC-ADUF membranes. The pure water fluxes of the membranes increase and then decrease as the RAC content increases. When the RAC content is 0.1 wt %, the pure water flux of the RAC-ADUF-0.1 membrane is 255.77 $L{\cdot}m^{-2}{\cdot}h^{-1}$, which is a 50% increase compared with the flux of the PSF membrane. The increased porosity and hydrophilicity of the PSF membrane caused by the addition of RAC prompted the improved water flux. When increasing the RAC content, the viscosity of the casting fluid will increase and the RAC may agglomerate, thus limiting the formation of macropores, reducing the transmembrane channels for water molecules

https://doi.org/10.1021/acsomega.2c04968
ACS Omega 2022, 7, 43829−43838

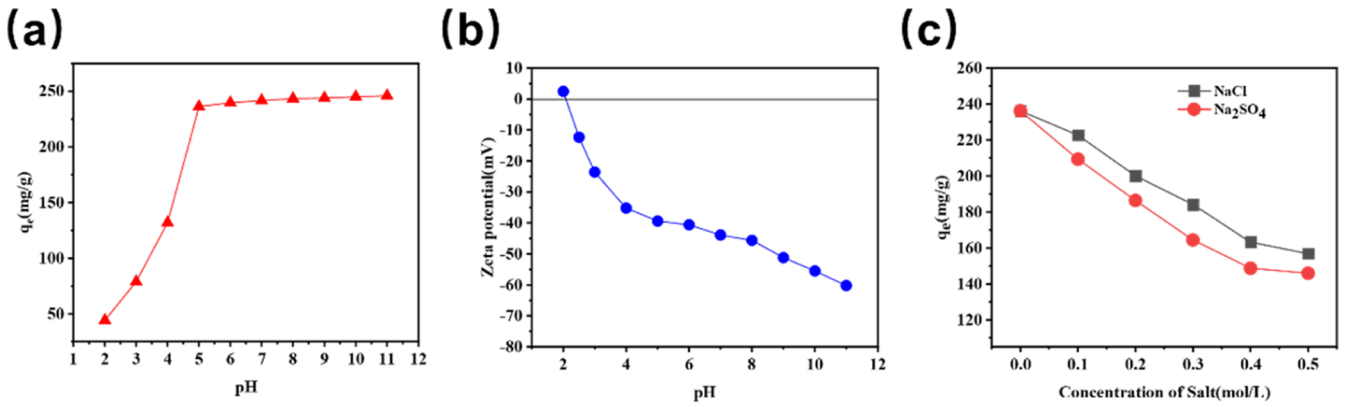

Figure 6. (a) Effect of pH on adsorption capacity of MB on RAC-ADU-0.1 membrane; (b) zeta potential of RAC-ADUF-0.1 membrane; and (c) effect of ionic strength on adsorption capacity of MB on RAC-ADU-0.1 membrane.

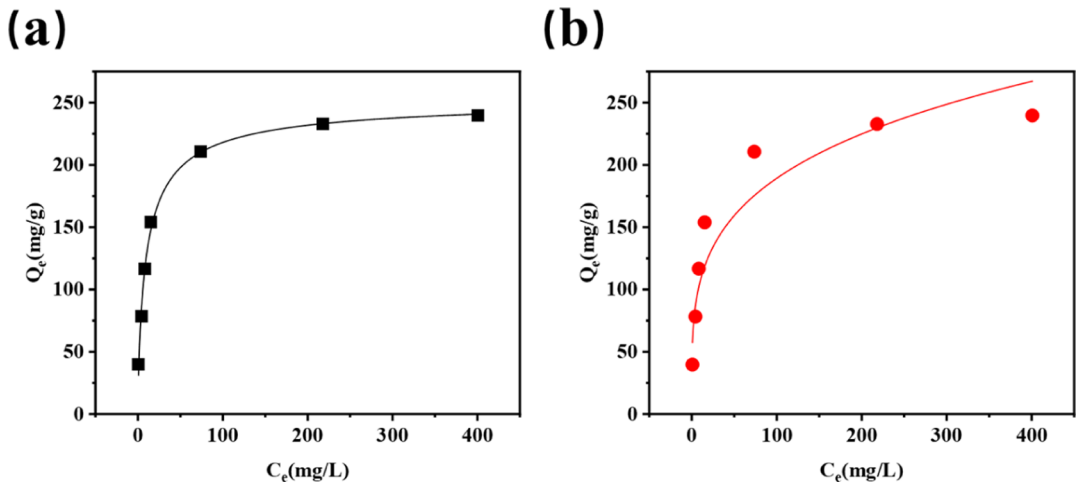

Figure 7. (a) Freundlich and (b) Langmuir isotherm plot for MB adsorbed on the RAC-ADUF-0.1 membrane.

and enhancing the transmembrane resistance.[40,45] Consequently, the water flux of the membrane reduces at higher RAC content. The rejection of BSA increased with the increase of RAC content, owing primarily to a reduction in the membrane pore size. When RAC content is 0.1%, the RAC-ADUF-0.1 membrane exhibits the highest pure water flux while maintaining excellent BSA rejection. Therefore, we selected the RAC-ADUF-0.1 membrane for the antifouling experiment, MB removal experiment, and regeneration experiment.

3.3. Antifouling Performance of RAC-ADUF-0.1 Membrane. We utilized the BSA solution to examine the antifouling performance of the RAC-ADUF-0.1 membrane (as shown in <u>Figure 5b,c</u>). After 1 h of filtration, the PSF membrane and the RAC-ADUF-0.1 membrane showed a decrease in flux due to further compaction, but the higher porosity and more hydrophilic RAC-ADUF-0.1 membrane exhibited a higher pure water flux. When the feed solution is replaced with BSA solution, the pure water flux decreased further due to membrane fouling. However, the flux of the RAC-ADUF-0.1 membrane was higher than that of the PSF membrane, indicating that the RAC-ADUF-0.1 membrane has superior antifouling performance to the PSF membrane. After washing the fouled membranes with pure water, the RAC-ADUF-0.1 membrane still exhibited a pure water flux of 237.03 $L \cdot m^{-2} \cdot h^{-1}$. By calculating the antifouling index (Figure 5c), the results showed that the RAC-ADUF-0.1 membrane had high flux recovery (91.14%), and a low reversible fouling (R_r) and irreversible fouling (R_{ir}), while the opposite was true for the PSF membrane. It can be obtained that the RAC-ADUF-0.1 membrane has excellent antifouling performance.[19] This is because the RAC-ADUF-0.1 membrane is more hydrophilic than PSF membranes, which causes water molecules on the membrane surface to form a hydration layer, thus exhibiting superior antifouling properties.[41]

3.4. Static Adsorption of MB by RAC-ADUF-0.1 Membrane. *3.4.1. Effects of pH and Interference Ions on Static Adsorption.* The solution pH affects the surface charge of the RAC-ADUF membrane, the dissociation of active site functional groups, and the structure of the dye. Therefore, the effect of pH on the adsorption of MB by the RAC-ADUF-0.1 membrane was investigated (Figure 6a). It is observed that the overall trend of equilibrium adsorption rises with increasing pH, and the growth rate gradually slows down for pH larger than 5. The effect of solution pH on the adsorption of MB by the membrane is mainly in two ways. One is to change the charge on the surface of the membrane, as seen by the zeta test (Figure 6b), with increasing pH the negative charge on the membrane surface increases due to the increased ionization of the surface carboxyl group into $-COO^-$.[11,46] Moreover, the form of the dye in the water has changed. MB is a cationic dye, and increasing pH value also promotes more ionization of MB into MB^+.[12] Therefore, changing the pH of the solution can help the RAC-ADUF-0.1 membrane to adsorb more methylene blue on the RAC-ADUF-0.1 membrane through

https://doi.org/10.1021/acsomega.2c04968
ACS Omega 2022, 7, 43829−43838

Table 3. Langmuir, Freundlich, and Dubinin−Radushkevich Isotherm Constants for MB Adsorption on the RAC-ADUF-0.1 Membrane

Langmuir model			Freundlich model				Dubinin−Radushkevich model		
q_m(mg/g)	K_L(mL/mg)	R^2	R_L	K_F(mg/g)	n	R^2	B	E	R^2
238.46	0.1194	0.99	0.077	60.3	0.248	0.895	0.07	2.67	0.934

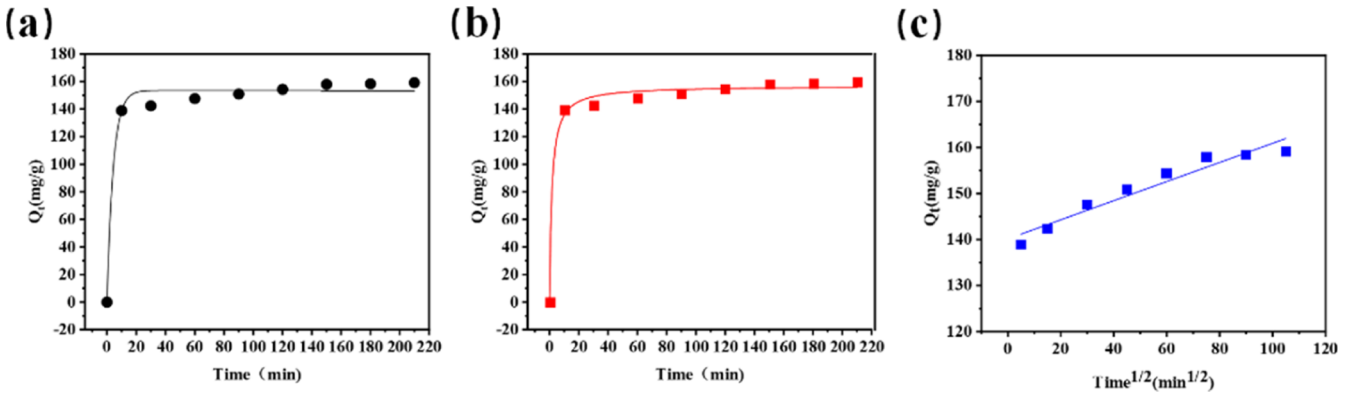

Figure 8. (a) Pseudo-first- and (b) pseudo-second-order kinetic and (c) Weber−Morris model for MB adsorption on the RAC-ADUF-0.1 membrane.

Table 4. Kinetic Parameters Obtained for MB Adsorption Using PFO, PSO Kinetic Model, and Weber−Morris Model

Pseudo-first-order kinetic model			Pseudo-second-order kinetic model			Weber−Morris model		
$q_{e,cal}$(mg/g)	k_1(min^{-1})	R^2	$q_{e,cal}$(mg/g)	k_2(g mg^{-1} h^{-1})	R^2	K_i(g mg^{-1} min$^{-0.5}$)	C(mg/g)	R^2
153.46	0.2332	0.986	156.81	0.00407	0.992	0.207	140.12	0.927

electrostatic interactions. Thus, the optimum pH condition for MB is 5. These conditions were used in subsequent experimental studies.

Dye wastewater contains large amounts of inorganic salt ions (NaCl and Na_2SO_4),[10] and the presence of inorganic salts can affect the adsorption process of dyes.[47,48] We tested the effect of NaCl and Na_2SO_4 on the adsorption MB of the RAC-ADUF-0.1 membrane, respectively, as shown in Figure 6c. It can be seen that the adsorption of the RAC-ADUF-0.1 membrane decreases with increasing concentration of the salt solution, this is because the presence of the inorganic salt weakens the electrostatic gravitational force between the adsorption active site and the dye molecules.[49] It can also be seen that Na_2SO_4 affects the adsorption process to a greater extent than NaCl at the same ionic concentration, as Na_2SO_4 carries more charge than NaCl.[50]

3.4.2. Adsorption Isotherm. To gain insights into the adsorption process, the characteristics of MB adsorption by the RAC-ADUF-0.1 membrane were further analyzed by Langmuir and Freundlich models. Based on the experimental data and the isotherms obtained from the nonlinear regression of the two models, as shown in Figure 7, the results demonstrated that the Langmuir isotherm model fitted the adsorption data better than the Freundlich model. This indicates that the adsorption sites on the RAC-ADUF-0.1 membrane may have similar adsorption energies, with dye molecules predominating in monolayer adsorption. In addition, the separation factors R_L of the Langmuir model were all less than 1[51] (Table 3), indicating the good performance of RAC-ADUF-0.1 adsorption MB. To deepen the understanding of the adsorption mechanism, we chose the D−R isotherm model to describe the adsorption on homogeneous and inhomogeneous surfaces, as shown in Table 3, the average adsorption energy (E) was less than 8 kJ/mol indicating that the adsorption process between RAC-ADUF-0.1 membrane and MB was mainly physical adsorption.[52]

3.4.3. Adsorption Kinetics. Adsorption is a physicochemical process of transferring a solute from the liquid phase to the surface of an adsorbent.[53] The adsorption of MB by RAC-ADUF-0.1 membrane was analyzed using pseudo-first-order (PFO), pseudo-second-order (PSO) and the Weber−Morris model. As shown in Figure 8, the removal rate of MB by the RAC-ADUF-0.1 membrane was quite fast (∼83%) at the beginning of the adsorption stage (0−10 min) and gradually reached the adsorption equilibrium state after about 60 min. This is primarily attributable to the presence of numerous empty adsorption sites on the RAC-ADUF-0.1 membrane during the early stages of adsorption,[54] and the remaining adsorption sites are difficult to be occupied over time due to the repulsive forces between the RAC-ADUF-0.1 membrane and the MB molecules.

The kinetic parameters and coefficients of determination (R^2) were determined by non-linear regression, as shown in Table 4. The R^2 values for the PSO kinetic model were closer to 1 compared to the PFO model, and the fitted data for the PSO model were close to the experimental data. Consequently, the PSO kinetic model more accurately describes the behavior of MB adsorption on the RAC-ADUF-0.1 membrane. We used the Weber−Morris model to analyze the rate-determining step of MB adsorption by the RAC-ADUF-0.1 membrane, as shown in Figure 8c, the fitted curve is linear and not passing through the origin, indicating that intraparticle diffusion is not the only rate control step and that external mass transfer may also be important in the rate control step due to the large intercept of the linear part of the plot. Thus, the whole adsorption process may be controlled by both external mass transfer and

https://doi.org/10.1021/acsomega.2c04968
ACS Omega 2022, 7, 43829−43838

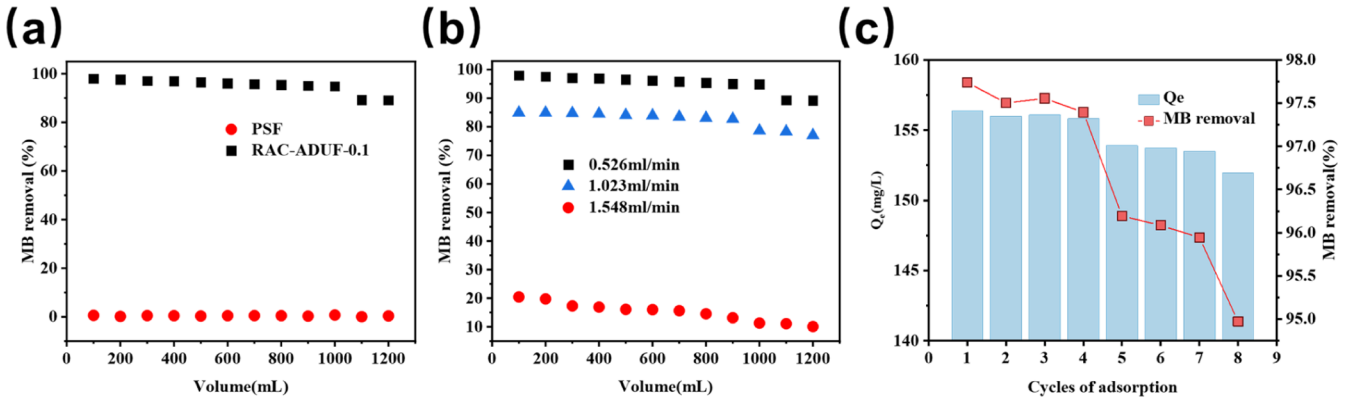

Figure 9. (a) Adsorption curves of MB on PSF and RAC-ADUF-0.1 membranes at fixed flow rates (0.526 mL/min); (b) adsorption curves of MB on RAC-ADUF-0.1 membranes at fixed flow rates (0.526, 1.025, and 1.548 mL/min); and (c) adsorption efficiency and adsorption capacity of RAC-ADUF-0.1 membrane after the adsorption−desorption cycle.

intraparticle diffusion, with intraparticle diffusion playing a dominant role in the control of the adsorption process.[47,49,52,55,56]

3.5. Adsorption of MB by Dynamic Filtration. To investigate the RAC-ADUF-0.1 membrane in practical operation applications, the membrane performance for MB removal was further investigated in continuous filtration. Figure 9a compares the removal efficiency of the PSF membrane and the RAC-ADUF-0.1 membrane for MB at a fixed flow rate (0.526 mL/min), and it can be seen that the removal efficiency of MB by PSF is almost 0. This is because the sieving mechanism of the UF membrane is mainly size sieving, and the MB molecular size is much smaller than that of the pore size of the UF membrane.[57] Therefore, MB can completely pass through the UF membrane. On the contrary, because RAC has a more excellent adsorption performance, the removal efficiency of MB by RAC-ADUF-0.1 membrane reaches 99%. In addition, the flow rate affects the mass-transfer process of MB to the adsorption sites during the dynamic filtration and adsorption process. Figure 9b reflects the removal efficiency of MB removal by adsorption of the RAC-ADUF-0.1 membrane at different flow rates. It can be seen that when the flow rate was 0.526 mL/min, the RAC-ADUF-0.1 membrane was able to reach about 98% of MB removal; however, when the flow rate was increased to 1.548 mL/min, the removal of MB by RAC-ADUF-0.1 membrane decreased to 15%. When the MB flow rate is faster making its residence time on the membrane shorter, it leaves the membrane before adsorption equilibrium occurs. Therefore, at higher flow rates, the RAC-ADUF-0.1 membrane cannot effectively remove MB.

3.6. Membrane Regeneration Performance. The regeneration and reuse of adsorption membranes are important factors in assessing their potential for practical applications. We employ anhydrous ethanol solutions to regenerate membranes after the adsorption of methamphetamine. The adsorption capacity and MB removal rate of the RAC-ADUF-0.1 membrane after the different numbers of iterations and regeneration using desorption are shown in Figure 9c. The adsorption efficiency and adsorption capacity of the RAC-ADUF-0.1 membrane for MB decreased gradually with the increase of cycles, but it still maintained more than 95% adsorption rate after eight adsorption−desorption cycles, indicating that the RAC-ADUF-0.1 membrane sowed excellent regeneration performance and has a greater potential for application in the treatment of dye wastewater.

4. CONCLUSIONS

In this study, AC was prepared from the reed rhizome residue (Chinese herbal medicine waste residue) and fixed in the UF membrane by phase inversion. The prepared RAC-ADUF membrane showed an excellent antifouling ability while maintaining excellent pure water flux (255.77 $L{\cdot}m^{-2}{\cdot}h^{-1}$) and BSA rejection (99.3%). The doping of RAC into the membrane provides the UF membrane surface with adsorption sites and a strong removal ability (99%) for MB. The analysis of the isothermal adsorption model and adsorption kinetic model demonstrated that the PSO kinetic model and Langmuir were more accurate to describe the adsorption process, and the adsorption mechanism was mostly pore filling. Meanwhile, the prepared RAC-ADUF membrane can also be reused, and the adsorption efficiency of MB can still be retained at about 95% after eight adsorption-regeneration experiments. In conclusion, the adsorption-separation dual-function ultrafiltration membrane was prepared by using Chinese herbal medicine waste residue as the raw material not only to resolve the environmental impact of waste herbs but also to reduce the environmental pollution of small-molecule organic dyes.

■ ASSOCIATED CONTENT

Supporting Information

The Supporting Information is available free of charge at https://pubs.acs.org/doi/10.1021/acsomega.2c04968.

Analysis of adsorption data, isotherm model, and kinetic model (PDF)

■ AUTHOR INFORMATION

Corresponding Author

Zhen Li − *School of Chemical Engineering and Technology, Tianjin University, Tianjin 300072, China; Department of Chemical Engineering, Tianjin Renai College, Tianjin 301636, China;* orcid.org/0000-0003-3221-8488; Email: jane_lee@tju.edu.cn

Authors

Xiongwei Luo − *Department of Chemical Engineering, Tianjin Renai College, Tianjin 301636, China*

https://doi.org/10.1021/acsomega.2c04968
ACS Omega 2022, 7, 43829−43838

Yonghong Li − *School of Chemical Engineering and Technology, Tianjin University, Tianjin 300072, China;* orcid.org/0000-0002-6406-165X

Complete contact information is available at: https://pubs.acs.org/10.1021/acsomega.2c04968

Author Contributions

Z.L.: conceptualization, investigation, formal analysis, visualization, validation, and writing original draft; X.L.: conceptualization, investigation, formal analysis, and validation; and Y.L.: funding acquisition, investigation, project administration, conceptualization, and supervision.

Notes

The authors declare no competing financial interest.

■ ACKNOWLEDGMENTS

We thank the National College Students Innovation and Entrepreneurship Training Program (202214038045 and 202214038040).

■ REFERENCES

(1) Nasrullah, A.; Saad, B.; Bhat, A. H.; Khan, A. S.; Danish, M.; Isa, M. H.; Naeem, A. Mangosteen peel waste as a sustainable precursor for high surface area mesoporous activated carbon: Characterization and application for methylene blue removal. *J. Clean. Prod.* **2019**, *211*, 1190−1200.

(2) Sonawane, G. H.; Shrivastava, V. S. Removal of hazardous dye from synthetic textile dyeing and printing effluents by Archis hypogaea L. shell: a low cost agro waste material. *Desalination Water Treat.* **2011**, *29*, 29−38.

(3) Ihsanullah, I.; Bilal, M.; Jamal, A. Recent Developments in the Removal of Dyes from Water by Starch-Based Adsorbents. *Chem. Rec.* **2022**, *22*, No. e202100312.

(4) Yilmaz, M.; Mengelizadeh, N.; Saloot, M. k.; shahbaksh, S.; Balarak, D. Facile synthesis of Fe3O4/ZnO/GO photocatalysts for decolorization of acid blue 113 under solar, visible and UV lights. *Mater. Sci. Semicond. Process.* **2022**, *144*, 106593.

(5) Mousavi, S. R.; Asghari, M.; Mahmoodi, N. M. Chitosan-wrapped multiwalled carbon nanotube as filler within PEBA thin film nanocomposite (TFN) membrane to improve dye removal. *Carbohydr. Polym.* **2020**, *237*, 116128.

(6) Oveisi, M.; Alinia Asli, M.; Mahmoodi, N. M. Carbon nanotube based metal-organic framework nanocomposites: Synthesis and their photocatalytic activity for decolorization of colored wastewater. *Inorg. Chim. Acta* **2019**, *487*, 169−176.

(7) Mahmoodi, N. M.; Oveisi, M.; Bakhtiari, M.; Hayati, B.; Shekarchi, A. A.; Bagheri, A.; Rahimi, S. Environmentally friendly ultrasound-assisted synthesis of magnetic zeolitic imidazolate framework - Graphene oxide nanocomposites and pollutant removal from water. *J. Mol. Liq.* **2019**, *282*, 115−130.

(8) Alamin, N.; Khan, A. S.; Nasrullah, A.; Iqbal, J.; Ullah, Z.; Din, I. U.; Muhammad, N.; Khan, S. Z. Activated carbon-alginate beads impregnated with surfactant as sustainable adsorbent for efficient removal of methylene blue. *Int. J. Biol. Macromol.* **2021**, *176*, 233−243.

(9) Cheng, S.; Zhao, S.; Xing, B.; Liu, Y.; Zhang, C.; Xia, H. Preparation of magnetic adsorbent-photocatalyst composites for dye removal by synergistic effect of adsorption and photocatalysis. *J. Clean. Prod.* **2022**, *348*, 131301.

(10) Rafaqat, S.; Ali, N.; Torres, C.; Rittmann, B. Recent progress in treatment of dyes wastewater using microbial-electro-Fenton technology. *RSC Adv.* **2022**, *12*, 17104−17137.

(11) Vishnu, D.; Dhandapani, B.; Authilingam, S.; Sivakumar, S. V. A Comprehensive Review of Effective Adsorbents Used for the Removal of Dyes from Wastewater. *Curr. Anal. Chem.* **2022**, *18*, 255−268.

(12) Ramutshatsha-Makhwedzha, D.; Mavhungu, A.; Moropeng, M. L.; Mbaya, R. Activated carbon derived from waste orange and lemon peels for the adsorption of methyl orange and methylene blue dyes from wastewater. *Heliyon* **2022**, *8*, No. e09930.

(13) Yagub, M. T.; Sen, T. K.; Afroze, S.; Ang, H. M. Dye and its removal from aqueous solution by adsorption: A review. *Adv. Colloid Interface Sci.* **2014**, *209*, 172−184.

(14) Lau, H. S.; Yong, W. F. Recent progress and prospects of polymeric hollow fiber membranes for gas application, water vapor separation and particulate matter removal. *J. Mater. Chem. A* **2021**, *9*, 26454−26497.

(15) Al-Musawi, T.; Zaidan, H.; Saloot, M. K.; Shahbaksh, S.; Balarak, D. Photocatalytic degradation of Acid Red 88 dye using Pd@TMU-16 metal organic framework. *Int. J. Environ. Anal. Chem.* **2022**, *22*, 1−17.

(16) Al-Musawi, T. J.; Mengelizadeh, N.; Taghavi, M.; Shehu, Z.; Balarak, D. Capability of copper-nickel ferrite nanoparticles loaded onto multi-walled carbon nanotubes to degrade acid blue 113 dye in the sonophotocatalytic treatment process. *Environ. Sci. Pollut. Res.* **2022**, *29*, 51703−51716.

(17) Almasian, A.; Mahmoodi, N. M.; Olya, M. E. Tectomer grafted nanofiber: Synthesis, characterization and dye removal ability from multicomponent system. *J. Ind. Eng. Chem.* **2015**, *32*, 85−98.

(18) Muthumareeswaran, M. R.; Agarwal, G. P. Feed concentration and pH effect on arsenate and phosphate rejection via polyacrylonitrile ultrafiltration membrane. *J. Membr. Sci.* **2014**, *468*, 11−19.

(19) Wen, X.; He, C.; Hai, Y.; Ma, R.; Sun, J.; Yang, X.; Qi, Y.; Wei, H.; Chen, J. Fabrication of an antifouling PES ultrafiltration membrane via blending SPSF. *RSC Adv.* **2022**, *12*, 1460−1470.

(20) Nasrullah, A.; Bhat, A. H.; Naeem, A.; Isa, M. H.; Danish, M. High surface area mesoporous activated carbon-alginate beads for efficient removal of methylene blue. *Int. J. Biol. Macromol.* **2018**, *107*, 1792−1799.

(21) Ahmadi, S.; Ganjidoust, H. Using banana peel waste to synthesize BPAC/ZnO nanocomposite for photocatalytic degradation of Acid Blue 25: Influential parameters, mineralization, biodegradability studies. *J. Environ. Chem. Eng.* **2021**, *9*, 106010.

(22) Aldawsari, A.; Ali Khan, M. A.; Hameed, B. H.; AlOthman, Z. A.; Raza Siddiqui, M. R.; Hadj Ahmed, A. Y. B. H.; Alsohaimi, I. H. Development of activated carbon from Phoenix dactylifera fruit pits: process optimization, characterization, and methylene blue adsorption. *Desalination Water Treat.* **2017**, *62*, 273−281.

(23) Gupta, V. K.; Mittal, A.; Malviya, A.; Mittal, J. Adsorption of carmoisine A from wastewater using waste materials-Bottom ash and deoiled soya. *J. Colloid Interface Sci.* **2009**, *335*, 24−33.

(24) Islam, M. A.; Sabar, S.; Benhouria, A.; Khanday, W. A.; Asif, M.; Hameed, B. H. Nanoporous activated carbon prepared from karanj (Pongamia pinnata) fruit hulls for methylene blue adsorption. *J. Taiwan Inst. Chem. Eng.* **2017**, *74*, 96−104.

(25) Ren, Y.; Li, T.; Zhang, W.; Wang, S.; Shi, M.; Shan, C.; Zhang, W.; Guan, X.; Lv, L.; Hua, M.; Pan, B. MIL-PVDF blend ultrafiltration membranes with ultrahigh MOF loading for simultaneous adsorption and catalytic oxidation of methylene blue. *J. Hazard. Mater.* **2019**, *365*, 312−321.

(26) Fang, X.; Li, J.; Li, X.; Pan, S.; Zhang, X.; Sun, X.; Shen, J.; Han, W.; Wang, L. Internal pore decoration with polydopamine nanoparticle on polymeric ultrafiltration membrane for enhanced heavy metal removal. *Chem. Eng. J.* **2017**, *314*, 38−49.

(27) Rana, D.; Narbaitz, R. M.; Garand-Sheridan, A.-M.; Westgate, A.; Matsuura, T.; Tabe, S.; Jasim, S. Y. Development of novel charged surface modifying macromolecule blended PES membranes to remove EDCs and PPCPs from drinking water sources. *J. Mater. Chem. A* **2014**, *2*, 10059−10072.

(28) Liao, Z.; Nguyen, M. N.; Wan, G.; Xie, J.; Ni, L.; Qi, J.; Li, J.; Schäfer, A. I. Low pressure operated ultrafiltration membrane with integration of hollow mesoporous carbon nanospheres for effective removal of micropollutants. *J. Hazard. Mater.* **2020**, *397*, 122779.

(29) He, J.; Matsuura, T.; Chen, J. P. A novel Zr-based nanoparticle-embedded PSF blend hollow fiber membrane for treatment of

arsenate contaminated water: Material development, adsorption and filtration studies, and characterization. *J. Membr. Sci.* **2014**, *452*, 433−445.
(30) Zhu, J.; Tian, M.; Zhang, Y.; Zhang, H.; Liu, J. Fabrication of a novel "loose" nanofiltration membrane by facile blending with Chitosan-Montmorillonite nanosheets for dyes purification. *Chem. Eng. J.* **2015**, *265*, 184−193.
(31) Ghaemi, N.; Madaeni, S. S.; Daraei, P.; Rajabi, H.; Zinadini, S.; Alizadeh, A.; Heydari, R.; Beygzadeh, M.; Ghouzivand, S. Polyethersulfone membrane enhanced with iron oxide nanoparticles for copper removal from water: Application of new functionalized Fe3O4 nanoparticles. *Chem. Eng. J.* **2015**, *263*, 101−112.
(32) Yurekli, Y. Removal of heavy metals in wastewater by using zeolite nano-particles impregnated polysulfone membranes. *J. Hazard. Mater.* **2016**, *309*, 53−64.
(33) Mukherjee, R.; Bhunia, P.; De, S. Impact of graphene oxide on removal of heavy metals using mixed matrix membrane. *Chem. Eng. J.* **2016**, *292*, 284−297.
(34) Li, X.; Fang, X.; Pang, R.; Li, J.; Sun, X.; Shen, J.; Han, W.; Wang, L. Self-assembly of TiO2 nanoparticles around the pores of PES ultrafiltration membrane for mitigating organic fouling. *J. Membr. Sci.* **2014**, *467*, 226−235.
(35) Ma, L.; Chen, J.; Wu, Z.; Tong, J.; Chen, Y. Research Progress of Biological Processing of Traditional Chinese Medicine Residues. *Lishizhen Med. Mater. Med. Res.* **2016**, *27*, 194−196.
(36) Shen, Q.; Wang, Z.; Yu, Q.; Cheng, Y.; Liu, Z.; Zhang, T.; Zhou, S. Removal of tetracycline from an aqueous solution using manganese dioxide modified biochar derived from Chinese herbal medicine residues. *Environ. Res.* **2020**, *183*, 109195.
(37) Li, Z.; Han, Q.; Zong, Z.; Xu, Q.; Wang, K. Exploring on the optimal preparation conditions of activated carbon produced from solid waste produced from sugar industry and Chinese medicine factory. *Waste Dispos. Sustain. Energy* **2020**, *2*, 65−77.
(38) Abdi, J.; Vossoughi, M.; Mahmoodi, N. M.; Alemzadeh, I. Synthesis of metal-organic framework hybrid nanocomposites based on GO and CNT with high adsorption capacity for dye removal. *Chem. Eng. J.* **2017**, *326*, 1145−1158.
(39) Hu, X.; Jia, L.; Cheng, J.; Sun, Z. Magnetic ordered mesoporous carbon materials for adsorption of minocycline from aqueous solution: Preparation, characterization and adsorption mechanism. *J. Hazard. Mater.* **2019**, *362*, 1−8.
(40) Liu, Q.; Huang, S.; Zhang, Y.; Zhao, S. Comparing the antifouling effects of activated carbon and TiO2 in ultrafiltration membrane development. *J. Colloid Interface Sci.* **2018**, *515*, 109−118.
(41) Zhang, R.; Liu, Y.; He, M.; Su, Y.; Zhao, X.; Elimelech, M.; Jiang, Z. Antifouling membranes for sustainable water purification: strategies and mechanisms. *Chem. Soc. Rev.* **2016**, *45*, 5888−5924.
(42) Miller, D. J.; Dreyer, D. R.; Bielawski, C. W.; Paul, D. R.; Freeman, B. D. Surface Modification of Water Purification Membranes. *Angew. Chem., Int. Ed.* **2017**, *56*, 4662−4711.
(43) Yu, L.-Y.; Xu, Z.-L.; Shen, H.-M.; Yang, H. Preparation and characterization of PVDF−SiO_2 composite hollow fiber UF membrane by sol−gel method. *J. Membr. Sci.* **2009**, *337*, 257−265.
(44) Yuan, S.; Zhang, G.; Zhu, J.; Mamrol, N.; Liu, S.; Mai, Z.; Van Puyvelde, P.; Van der Bruggen, B. Hydrogel assisted interfacial polymerization for advanced nanofiltration membranes. *J. Mater. Chem. A* **2020**, *8*, 3238−3245.
(45) Leo, C. P.; Ahmad Kamil, N. H.; Junaidi, M. U. M.; Kamal, S. N. M.; Ahmad, A. L. The potential of SAPO-44 zeolite filler in fouling mitigation of polysulfone ultrafiltration membrane. *Sep. Purif. Technol.* **2013**, *103*, 84−91.
(46) Wang, X.; Baker, J.; Carlson, K.; Li, Z. Mechanisms of Selected Anionic Dye Removal by Clinoptilolite. *Crystals* **2022**, *12*, 727.
(47) Al-Musawi, T. J.; Mengelizadeh, N.; Al Rawi, O.; Balarak, D. Capacity and Modeling of Acid Blue 113 Dye Adsorption onto Chitosan Magnetized by Fe2O3 Nanoparticles. *J. Polym. Environ.* **2022**, *30*, 344−359.
(48) Sriram, G.; Bendre, A.; Mariappan, E.; Altalhi, T.; Kigga, M.; Ching, Y. C.; Jung, H.-Y.; Bhaduri, B.; Kurkuri, M. Recent trends in the application of metal-organic frameworks (MOFs) for the removal of toxic dyes and their removal mechanism-a review. *Sustainable Mater. Technol.* **2022**, *31*, No. e00378.
(49) Balarak, D.; Zafariyan, M.; Igwegbe, C. A.; Onyechi, K. K.; Ighalo, J. O. Adsorption of Acid Blue 92 Dye from Aqueous Solutions by Single-Walled Carbon Nanotubes: Isothermal, Kinetic, and Thermodynamic Studies. *Environ. Processes* **2021**, *8*, 869−888.
(50) Jin, J.; Du, X.; Yu, J.; Qin, S.; He, M.; Zhang, K.; Chen, G. High performance nanofiltration membrane based on SMA-PEI cross-linked coating for dye/salt separation. *J. Membr. Sci.* **2020**, *611*, 118307.
(51) Ho, Y. S.; McKay, G. Sorption of dye from aqueous solution by peat. *Chem. Eng. J.* **1998**, *70*, 115−124.
(52) Ma, J.; Yu, F.; Zhou, L.; Jin, L.; Yang, M.; Luan, J.; Tang, Y.; Fan, H.; Yuan, Z.; Chen, J. Enhanced Adsorptive Removal of Methyl Orange and Methylene Blue from Aqueous Solution by Alkali-Activated Multiwalled Carbon Nanotubes. *ACS Appl. Mater. Interfaces* **2012**, *4*, 5749−5760.
(53) El-Geundi, M. S. Adsorbents for industrial pollution control. *Adsorpt. Sci. Technol.* **1997**, *15*, 777−787.
(54) Ghaedi, M.; Shokrollahi, A.; Tavallali, H.; Shojaiepoor, F.; Keshavarz, B.; Hossainian, H.; Soylak, M.; Purkait, M. K. Activated carbon and multiwalled carbon nanotubes as efficient adsorbents for removal of arsenazo(III) and methyl red from waste water. *Toxicol. Environ. Chem.* **2011**, *93*, 438−449.
(55) Al-Degs, Y. S.; El-Barghouthi, M. I.; Issa, A. A.; Khraisheh, M. A.; Walker, G. M. Sorption of Zn(II), Pb(II), and Co(II) using natural sorbents: Equilibrium and kinetic studies. *Water Res.* **2006**, *40*, 2645−2658.
(56) Doğan, M.; Abak, H.; Alkan, M. Adsorption of methylene blue onto hazelnut shell: Kinetics, mechanism and activation parameters. *J. Hazard. Mater.* **2009**, *164*, 172−181.
(57) Konno, H.; Tsukada, A. Size- and ion-selective adsorption of organic dyes from aqueous solutions using functionalized UiO-66 frameworks. *Colloids Surf., A* **2022**, *651*, 129749.

https://doi.org/10.1021/acsomega.2c04968
ACS Omega 2022, 7, 43829−43838